HHS Public Access

Author manuscript

Cell Rep. Author manuscript; available in PMC 2018 April 19.

Published in final edited form as:

Cell Rep. 2018 March 20; 22(12): 3251–3264. doi:10.1016/j.celrep.2018.02.097.

Gcn4-Mediator Specificity Is Mediated by a Large and Dynamic Fuzzy Protein-Protein Complex

Lisa M. Tuttle[1,2], **Derek Pacheco**[1], **Linda Warfield**[1], **Jie Luo**[3], **Jeff Ranish**[3], **Steven Hahn**[1,*], and **Rachel E. Klevit**[2,4,*]

[1]Division of Basic Sciences, Fred Hutchinson Cancer Research Center, Seattle, WA 98109, USA

[2]Department of Biochemistry, University of Washington, Seattle, WA 98195, USA

[3]The Institute for Systems Biology, Seattle, WA 98109, USA

Summary

Transcription activation domains (ADs) are inherently disordered proteins that often target multiple coactivator complexes, but the specificity of these interactions is not understood. Efficient transcription activation by yeast Gcn4 requires its tandem ADs and four activator-binding domains (ABDs) on its target, the Mediator subunit Med15. Multiple ABDs are a common feature of coactivator complexes. We find that the large Gcn4-Med15 complex is heterogeneous and contains nearly all possible AD-ABD interactions. Gcn4-Med15 forms via a dynamic fuzzy protein-protein interface, where ADs bind the ABDs in multiple orientations via hydrophobic regions that gain helicity. This combinatorial mechanism allows individual low-affinity and specificity interactions to generate a biologically functional, specific, and higher affinity complex despite lacking a defined protein-protein interface. This binding strategy is likely representative of many activators that target multiple coactivators, as it allows great flexibility in combinations of activators that can cooperate to regulate genes with variable coactivator requirements.

Graphical abstract

In Brief: Tuttle et al. report a “fuzzy free-for-all” interaction mechanism that explains how seemingly unrelated transcription activators converge on a limited number of coactivator targets. The mechanism provides a rationale for the observation that individually weak and low-specificity interactions can combine to produce biologically critical function without requiring highly ordered structure.

*Correspondence: shahn@fredhutch.org (S.H.), klevit@u.washington.edu (R.E.K.).
[4]Lead Contact

SUPPLEMENTAL INFORMATION

Supplemental Information includes Supplemental Experimental Procedures, six figures, and three tables and can be found with this article online at https://doi.org/10.1016/j.celrep.2018.02.097.

AUTHOR CONTRIBUTIONS

L.M.T., S.H., and R.E.K. designed the research. L.M.T., D.P., L.W., J.L., and S.H. performed the experiments. L.M.T., D.P., L.W., J.L., J.R., S.H., and R.E.K. analyzed data. L.M.T., D.P., L.W., J.R., S.H., and R.E.K. wrote the paper.

DECLARATION OF INTERESTS

The authors declare no competing interests.

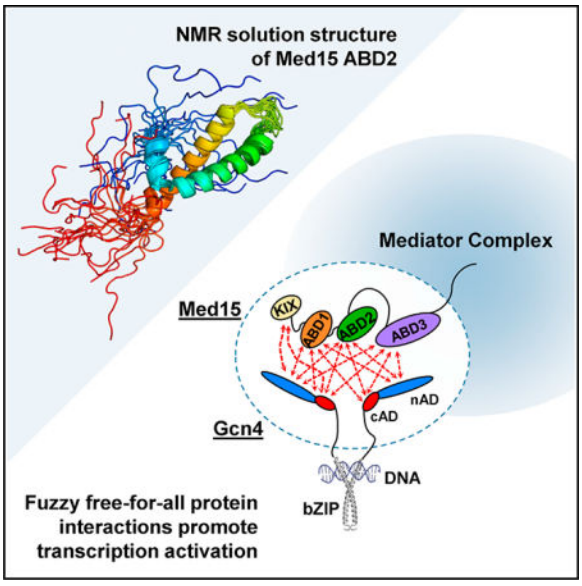

INTRODUCTION

Transcription activators lie at the endpoint of signaling pathways that control transcription in response to development, cell growth, stress, and other physiological signals (Levine et al., 2014; Spitz and Furlong, 2012). A central challenge in understanding gene regulation is to determine the mechanism and specificity of activators. Transcription activation domains (ADs) are intrinsically disordered, lack a stable structure in the absence of a binding partner, and do not share obvious primary sequence similarity (Dyson and Wright, 2005; Hahn and Young, 2011; Nguyen Ba et al., 2012; Tantos et al., 2012; Tompa et al., 2014). Most known activators work by targeting transcription co-activator complexes to stimulate both transcription preinitiation complex (PIC) assembly and chromatin modifications (Hahn and Young, 2011; Weake and Workman, 2010). For over thirty years, a central mystery surrounding transcriptional activators, once referred to as “acidic blobs and negative noodles” (Sigler, 1988), has been: how do activators specifically target unrelated coactivators?

The acidic transcription activator Gcn4 from *S. cerevisiae* has properties common to many eukaryotic activators. Gcn4 contains tandem intrinsically disordered ADs (tADs) that target coactivators, including Mediator, SAGA, Swi/Snf, and/or NuA4 to regulate a large number of genes in response to metabolic stress (Brown et al., 2001a; Brzovic et al., 2011; Drysdale et al., 1995; Fishburn et al., 2005; Herbig et al., 2010; Jackson et al., 1996; Jedidi et al., 2010; Natarajan et al., 2001; Qiu et al., 2016; Swanson et al., 2003; Warfield et al., 2014; Yoon et al., 2003). A key Gcn4 target is Med15/Gal11, a component of the Mediator tail module (Brzovic et al., 2011; Herbig et al., 2010; Jedidi et al., 2010; Warfield et al., 2014). Within its N-terminal half, Med15 contains four structured domains: a KIX domain (Novatchkova and Eisenhaber, 2004; Yang et al., 2006) and activator-binding domains (ABDs) 1; 2; and 3 that are recognized by Gcn4 (Herbig et al., 2010; Jedidi et al., 2010; Figure 1A). Although interactions have been detected between single-AD sequences and

individual ABDs, no single AD-ABD interaction is sufficient for efficient stimulation of transcription; high levels of activation are achieved only with the complete Med15 activator-binding region and the tandem Gcn4 ADs (Herbig et al., 2010; Jedidi et al., 2010). This implies that a single AD-ABD interaction lacks sufficient affinity and/or specificity to promote transcription.

The use of multiple ADs and ABDs is not unique to Gcn4 and Med15. Other strong activators, such as VP16 and p53, contain tandem ADs, and coactivators, such as CBP, Swi/Snf, and SAGA/NuA4, all contain multiple ABDs (Brown et al., 2001b; Chang et al., 1995; Díaz-Santín et al., 2017; Ferreon et al., 2009; Langlois et al., 2008; Prochasson et al., 2005; Regier et al., 1993; Unger et al., 1992; Walker et al., 1993). For example, multiple Gcn4 binding sites have been implicated in the SAGA/NuA4 activator-binding subunit Tra1, and inactivation of any one site leads to reduced factor recruitment at Gcn4-dependent genes (Díaz-Santín et al., 2017; Knutson and Hahn, 2011). Likewise, optimum activator-Swi/Snf binding and Swi/Snf recruitment requires both ABDs within the Swi5 and Swi1 subunits of Swi/Snf (Ferreira et al., 2009; Prochasson et al., 2003). Whereas multiple ADs and ABDs appears to be a common theme in transcriptional regulation, the mechanism of how a multiplicity of AD-ABD interactions give rise to the affinity and specificity required for AD function remains undefined.

We previously showed that the Gcn4 central AD (cAD) binds to ABD1 with a fuzzy protein-protein interface. Disordered on its own, cAD binds in multiple orientations to a shallow groove on ABD1, mediated almost entirely by hydrophobic interactions (Brzovic et al., 2011). Because a single AD-ABD interaction is not sufficient for transcription activation (Herbig et al., 2010), an important question arising from our findings is whether a fuzzy binding mode is retained in the larger physiological Gcn4-Med15 complex with its full complement of ADs and ABDs. An alternative model predicts that multiple ADs and ABDs will lock into a specific, more stable complex with higher affinity binding and conventional protein-protein interfaces. Indeed, in two systems involving intrinsically disordered proteins (IDPs) and structured binding partners that have been characterized at a structural level, the IDPs form heterogeneous complexes with individual interacting partners but form stable distinct higher ordered structures when all binding partners are present (Dyson and Wright, 2016; Saio et al., 2014). Such examples illustrate the importance of examining large natural complexes of IDPs and their targets. The distinction between the two possible mechanisms has important implications for which AD sequences can function together and the specificity of AD targets. A fuzzy binding mechanism is predicted to allow greater flexibility in AD-AD and AD-ABD combinations compared to systems that lock into a specific complex.

To determine whether the Gcn4-Med15 complex forms a large complex with specific contacts or interacts via a large fuzzy interface, we characterized the interactions between the Gcn4 tADs and the four ABDs of Med15, both individually and as part of the larger Gcn4-Med15 complex. Our data demonstrate that the presence of multiple binding components leads to a large gain in the affinity of Gcn4-Med15 binding but does not lead to formation of a distinct ordered structure. The functional complex is a dynamic fuzzy “free-for-all” involving hydrophobic patches of the tADs with ABD 1–3 and the KIX domain. Our results provide a general model for the mechanism of many activators that functionally bind

coactivators with multiple ABDs and demonstrate how multiple weak fuzzy interactions synergize to generate a biologically functional and specific interaction without adopting a unique protein-protein interface.

RESULTS

Both Gcn4 ADs Interact with All Individual Med15 ABDs

As a first step in characterization of the complete Gcn4-Med15 complex, we examined regions required for AD function and investigated the affinity of the individual and higher order AD-ABD interactions. The two Gcn4 ADs are the N-terminal (nAD; residues 1–100) and central (cAD; residues 101–134; Drysdale et al., 1995; Figure 1A). cAD is one of the shortest ADs known, with most of its function contained in a five-residue sequence motif WxxLF (residues 120–124; Warfield et al., 2014). In contrast, nAD function is dependent on clusters of hydrophobic residues located throughout residues 1–100 (Jackson et al., 1996). As AD function is usually confined to much shorter sequences, we examined whether any of the individual hydrophobic regions within nAD have function and whether any non-hydrophobic regions of nAD contribute to activity. A series of deletions and alanine substitutions was made within a Gcn4 derivative lacking the cAD, and function was measured at *ARG3* and *HIS4*, two Gcn4-dependent yeast genes (Figure S1). Consistent with prior results (Jackson et al., 1996), we found that Gcn4 nAD function requires four short hydrophobic regions (residues 4–16, 40–49, 65–69, and 94–98). We also found that residues between the clusters can be deleted with little or no detrimental effect. In several cases, deletions increase activity: deletion of residues between the first three hydrophobic regions to create one long hydrophobic region generates an AD with up to 4.6-fold higher activity relative to wild-type. Importantly, no individual short hydrophobic region has substantial activity when fused to the Gcn4 DNA-binding domain. Therefore, nAD function arises from multiple short non-redundant hydrophobic clusters with little or no inherent activity that together generate AD function.

We used isothermal calorimetry (ITC) and/or fluorescence polarization (FP) to measure the binding affinity of each AD and individual ABD and of a tAD-ABD1,2,3 complex (Table 1). With one exception, the individual pairwise interactions between individual nAD and cAD peptides and individual Med15 ABDs have similar low/modest affinities (K_d values of ~3–20 μM). The exception is cAD binding to ABD2, which is ~10-fold weaker (150 μM K_d). Although the Med15 KIX domainis as important functionally for Gcn4 activation as any other ABD (Herbig et al., 2010), neither nAD nor cAD showed detectable KIX binding in our assays. The tandem AD polypeptide (Gcn4 residues 1–134) binds to each individual ABD with an affinity close to the stronger of the individual nAD or cAD interactions, suggesting that the individual Gcn4 ADs bind to the same or overlapping sites on the ABDs. A striking gain in affinity is observed when tAD binds to longer Med15 polypeptides containing multiple ABDs (ABD123 and KIX123). For example, tAD binding to ABD123 (ABD1, ABD2, and ABD3 connected by short linkers) is about 20-fold higher affinity than the strongest piecemeal interaction, signifying that, when all domains are present, more than one ABD simultaneously contributes to binding. Notably, the presence of KIX along with ABD1,2,3 (KIX123) increases Gcn4 affinity by ~30%. Altogether, the results show that

multiple weak AD-ABD and KIX interactions in the full-length proteins combine to yield a much higher affinity Gcn4-Med15 interaction—in agreement with *in vivo* activation function.

A Heterogeneous Gcn4-Med15 Complex

A prediction of the fuzzy complex model for Gcn4-Med15 is that a complex containing multiple ADs and ABDs will not contain fixed protein-protein interactions and that individual ADs will sample multiple ABDs in different orientations, as was observed for cAD-ABD1 (Brzovic et al., 2011). The alternative "locked down" model predicts that specific protein-protein interactions will be adopted in the larger complexes. To test the two models, we used chemical crosslinking analyzed by mass spectrometry to detect interactions between the Gcn4 tAD and Med15 ABD123 or KIX123 (Figures 1B and 1C). Complexes of Gcn4 residues 1–140 (tAD) with either of the two Med15 constructs were treated with the zero-length crosslinker 1-ethyl-3-(3-dimethyla-minopropyl)carbodiimide hydrochloride (EDC) that links amine groups, such as those found in lysine side chains, to carboxylate groups, such as those found in the side chains of acidic amino acids. Identified crosslinks are summarized in Figures 1B and 1C and reported in Tables S1 and S2.

Crosslinks were observed between both ADs of Gcn4 and all four defined structural regions of Med15 (KIX domain and ABD1, 2, and 3) with one exception: no crosslinks between Gcn4 cAD and Med15 ABD3 were detected. In addition, fewer crosslinks were identified between the Gcn4 nAD and ABD3 than those involving the other subdomains, despite a similar number of potential crosslinking sites and the stronger intrinsic affinity of ABD3 compared to ABD2 (Table 1). The KIX domain, with little or no detectable binding to Gcn4 on its own, crosslinks extensively to Gcn4 in the large complex, mainly to nAD. Notably, the crosslink patterns between ABD1–3 and tAD are unchanged when the KIX domain is also present (KIX123 compared to ABD123). Thus, the crosslinking data show that KIX interacts directly with Gcn4, consistent with functional assays showing that KIX is as important as the individual ABD1, 2, and 3 domains for Gcn4 activation (Herbig et al., 2010). The results reveal that interactions involving the weaker binding domains of Med15 occur even when all domains are present, i.e., no domain outcompetes the others for AD binding. Such a mechanism predicts transient binding for each AD-ABD/KIX interaction.

tAD-Med15 Interactions Are a Sum of the Individual nAD and cAD Interactions

Together, the crosslinking and binding assays indicate that, whereas the large Gcn4-Med15 complex has high affinity, it is nevertheless heterogeneous. Two models are consistent with this behavior: (1) each AD binds each ABD/KIX with a dynamic and fuzzy protein-protein interface or (2) AD-ABD binding is dynamic, but individual AD-ABD binding occurs with unique non-fuzzy interfaces. To distinguish between these models, we investigated the properties of the individual AD-ABD complexes by nuclear magnetic resonance (NMR) and compared the results to those of the complete complex.

We first examined the environment of the polypeptide backbones of nAD, cAD, and tAD upon Med15 binding. Titrations were carried out for each combination of ^{13}C,^{15}N-labeled nAD, cAD, and tAD binding to unlabeled ABD1, ABD2, ABD3, and ABD123. In these

experiments, effects on the isotopically labeled component due to binding the non-labeled (silent) component are observed in (^{1}H,^{15}N)- and (^{1}H,^{13}C)-heteronuclear single quantum coherence (HSQC) spectra. Titrations were taken to full saturation where possible, based on measured K_d values (Table 1).

In each titration series, NMR peaks for affected residues changed their resonance position continuously as a function of added binding partner until saturation was reached (e.g., Figure S2). The chemical shift perturbation (CSP) of a peak was calculated as the difference in its chemical shift in the spectrum of free AD and in the most saturated spectrum. CSPs can reflect a change in local environment as from a gain in secondary structure and/or from the change in electronic environment due to the proximity of a binding partner or through allosteric effects and are generally a strong proxy for assessing binding interactions. CSPs for AD backbone amide (NH) groups are displayed as histograms in Figure 2, with a panel for each individual ABD (Figures 2A–2C) and a panel for the combined ABD123 (Figures 2D and S3A). Previously reported results for ^{15}N-cAD:ABD1 are included here for a complete comparison (Brzovic et al., 2011). Several general features emerge from the large body of data. First, perturbations occur in hydrophobic residue clusters along the AD sequence that correspond to the previously identified hydrophobic regions in Gcn4. Second, the same clusters are perturbed regardless of which ABD has been added. Third, in all cases, the fourth nAD hydrophobic cluster (residues 94–98) shows the largest CSPs, followed by the cAD cluster (residues 120–124), with smaller shifts in each of the other hydrophobic regions. Fourth, there are no new perturbations associated with tAD binding to Med15; both the identity and magnitudes of the CSPs observed in the isolated nAD and cAD are retained in full-length tAD (Figures 2, S3A, and S3B). Thus, we find no additional cryptic interaction sites in the full-length Gcn4 tandem AD.

Whereas the same regions of the ADs show CSPs when binding to all ABDs, the magnitudes of the shifts depend on the ABD binding partner. The contribution of each cluster is parsed out in Figure S3B, in which the maximum CSPs in each cluster are compared. Two clusters dominate the binding to all ABDs: one in the nAD and cAD. The other nAD clusters contribute differently depending on the ABD: the larger CSPs for the weaker hydrophobic regions in the ABD2 and ABD3 titrations suggest that these clusters play a larger role in ABD2 and ABD3 binding than in ABD1. The CSPs of the weakly interacting hydrophobic regions of nAD do not increase in the full-length complex, as might occur if a sequential binding mechanism were in play. Instead, the CSPs in tAD:ABD123 resemble the component tAD:ABD complexes, indicating that the importance of the weaker hydrophobic clusters for activator function is not a result of new or stabilized interactions in the full-length AD-ABD complex.

To further define the dynamic interface of Gcn4, we measured ^{15}N-relaxation parameters for nAD and nAD:ABD1. An increase in the transverse relaxation rate, R_2 (= $1/T_2$), upon binding is indicative of a role in binding for the affected residues (Delaforge et al., 2018). Upon binding ABD1, each of the hydrophobic regions of nAD shows an increase in R_2, supporting the direct involvement of these regions in binding ABD1 (Figures 2E and S3C). Notably, even region 65–69, which exhibits only very small CSPs, has elevated R_2 values upon binding ABD1. Consistent with the CSPs, the region of nAD including residues 94–98

shows the largest increase in R_2. Residues ~20–38 show no change in R_2 upon binding ABD1, which is consistent with transcription activity data that show residues in this region do not positively contribute to activity.

Gcn4 ADs Become Helical upon Binding Med15 ABDs

The primary interacting regions of many ADs become helical upon binding to their targets; e.g., residues 117–125 in Gcn4 cAD adopt helical structure upon ABD1 binding (Brzovic et al., 2011). We used the chemical shifts of free and bound nAD and cAD to assess secondary structure upon binding to Med15 ABDs (Tamiola and Mulder, 2012). Unbound nAD and cAD are completely disordered on their own, but each gains substantial helical content upon binding ABD1 (Figure S3D). The two most C-terminal hydrophobic clusters gain the most helicity: the nAD cluster exhibits up to 50% helical content, and the cAD cluster exhibits about 30%, whereas each of the other three nAD hydrophobic clusters show some helical character (<20%) upon binding ABD1. These analyses were performed on the two individual ADs where the most complete resonance assignments are available. However, chemical shifts in the tAD essentially match the component shifts of nAD and cAD (Figure 2), allowing us to conclude that the same pattern and magnitude of helical structure is gained when tAD binds to ABD1.

Secondary structure gained by nAD upon binding to ABD2 qualitatively resembles that of nAD:ABD1, except that the C-terminal hydrophobic cluster shows only ~25% helical content (Figure S3D). This analysis was performed for spectra collected under saturating concentrations of each ABD, so the differences in estimated helicity of residues 94–98 suggest either that the cluster spends less time bound to ABD2 than it does to ABD1 (i.e., has a faster off rate) and/or that it binds to ABD2 in non-helical as well as helical conformations. Overall, our analysis shows that (1) hydrophobic regions of ADs that interact with ABDs gain helical content upon binding and (2) the most frequent AD-ABD contacts are with Gcn4 hydrophobic clusters 94–98 and 120–124. Nevertheless, the other nAD hydrophobic clusters play an essential functional role (Figure S1) and contribute significantly to the overall interaction with Med15.

Structure of Med15 ABD2

Unlike the ADs, which are intrinsically disordered in their free states, ABDs typically adopt defined three-dimensional structures, though few ABD structures have been experimentally determined. We set out to determine structures for Med15 ABD2 (residues 277–368) and ABD3 (residues 484–651). Whereas NMR analysis showed that ABD3 is largely structured in the absence of AD binding (not shown), this domain has neither the solubility nor stability properties required for a full structure determination by NMR. In contrast, ABD2 was tractable for structure determination in its free state. Backbone and side-chain resonance assignments for $^{13}C,^{15}N$-ABD2 were determined with overall completeness of 72% (Table S3). The chemical shifts predict that ABD2 contains three α helices (Figures 3 and S4B). A solution structure calculated using chemical shifts, nuclear overhauser effects (NOEs), and N-H residual dipolar couplings (RDCs) as experimental constraints is well defined, with a backbone root-mean-square deviation (RMSD) of 0.7 Å for the ordered regions (amino acids

[aas] 293–322 and 328–354) in the top 20 of 200 total generated structures (Figure 3A; PDB 6ALY).

ABD2 is composed of three α helices: α1 (aas 292–299); α2 (aas 303–323); and α3 (aas 330–354) with disordered N- and C-terminal tails (Figures 3A and S4B). Unlike ABD1 that binds cAD via a shallow hydrophobic groove (Brzovic et al., 2011), ABD2 has no obvious groove but instead has two hydrophobic surface patches (Figure 3B). One hydrophobic patch is created at the interface of α2 and α3 and is defined by the near stacking of three aromatic residues (F319, F330, and Y340). A second elongated patch includes α1 and spirals around the ABD2 structure. The ABD2 construct contains 18 charged residues, with a net positive charge of +4. A patch of positive charge separates the two hydrophobic patches (shown as blue; Figure 3C). The structure reveals that although ABD1 and ABD2 are both primarily composed of helices, helical ABDs do not conform to a single structural motif.

ABD1 and ABD2 Use Similar Strategies to Bind ADs of Different Sequence

To identify the AD-binding site(s) on the ABDs, we performed NMR titration experiments for each combination of ^{13}C,^{15}N-labeled ABD1 and ABD2 with unlabeled nAD, cAD, and tAD. We showed previously that cAD binds to ABD1 in a shallow hydrophobic groove as a fuzzy cAD-ABD1 complex (Brzovic et al., 2011). Remarkably, the CSPs in ABD1 are nearly identical, regardless of the AD binding partner (Figures 4A, 4C, and S4C). The similar CSP patterns induced upon binding to each of the three AD variants indicate that their interaction interface is essentially the same. Consistent with this, in a competition binding experiment in which unlabeled cAD was added to ^{15}N-tAD + ABD1, all ^{15}N-tAD peaks returned toward their chemical shifts in the unbound tAD spectrum, indicating that cAD can compete off both cAD and nAD residues (Figure S3E). The simplest explanation for these combined observations is that ABD1 does not bind the different ADs with a sequence-specific interface but rather as a “cloud” of hydrophobic character. This model is completely consistent with our earlier characterization of the fuzzy cAD-ABD1 complex.

ABD2 has substantially weaker affinity for cAD than for either nAD or tAD, suggesting that there may be different modes of ABD2 binding. Nevertheless, we again observe highly similar CSPs within ABD2 upon binding the nAD, cAD, and tAD peptides (Figures 4B, 4D, and S4D). The CSPs are widespread, with the largest perturbations occurring in/near the two ABD2 hydrophobic patches, regardless of whether nAD, cAD, or tAD is binding. Therefore, ABD1 and ABD2 each accommodate their AD binding partner(s) in a manner that is independent of the specific sequence of the AD, consistent with a fuzzy binding interface. However, ABD1 contains a single predominant binding groove, whereas two hydrophobic binding surfaces on ABD2 yield a less localized interaction that may explain the lower affinity for AD-ABD2 binding.

ABD1 and ABD2 Bind ADs with a Fuzzy Interface

In our previous studies, the definitive evidence for fuzzy binding of cAD-ABD1 derived from NMR spin-label experiments through measurement of paramagnetic relaxation enhancement (PRE) (Brzovic et al., 2011; Warfield et al., 2014). These studies showed that the cAD peptide bound ABD1 in multiple orientations. We performed analogous

experiments using a series of nAD, cAD, and tAD constructs, to which a single paramagnetic spin-label probe (4-(2-iodoacetamido)-TEMPO) was attached at sites near, but not in, a primary interacting region. Gcn4 residues T82, T105, and S117 were individually mutated to Cys to allow chemical attachment of the spin-label probe (Figure 5A). Groups that are close to a paramagnetic probe will suffer loss of peak intensity, quantified as I_{para}/I_{dia}, where I_{dia} (diamagnetic) is the reference intensity after reduction of the paramagnetic probe with ascorbic acid (see Figure S5 for ^{13}C-HSQC spectra). If there is a preferred orientation of an AD in the AD-ABD complex, we expect different patterns of intensity loss when the spin label is on opposite ends of the AD peptide. We collected (^{1}H,^{15}N)- and (^{1}H, ^{13}C)-HSQC spectra for ABD1 and ABD2 with each of the spin-labeled ADs at ~50% saturation and plotted the location of intensity loss for NH and CH groups on the structures of ABD1 and ABD2 (Figures 5C and 5D, respectively). In every case, the observed patterns of intensity loss are highly similar, regardless of which TEMPO-AD was added (Figures 5B, S5B, and S6). The results indicate that the AD hydrophobic clusters bind without any discernable orientation bias, either when presented as individual ADs or when both nAD and cAD are present in the tandem construct. Altogether, the results fit a model in which fuzzy binding interfaces are used by each ABD-AD interaction. Because our results above showed that the interactions of tAD with ABD1 and ABD2 are equivalent in the individual and larger complex, we conclude that the AD-ABD interactions in the larger complex are also fuzzy. Using this mechanism for binding allows the multiple hydrophobic clusters in tAD to increase binding affinity through avidity but neither limits nor alters the possible ensemble of complexes that simultaneously exist.

DISCUSSION

A long-standing challenge in gene regulation has been to understand how seemingly unrelated transcription activators converge on a limited number of coactivator targets. This situation also raises the question of specificity in activator-coactivator interactions. For example, the fuzzy binding interface of the Gcn4 cAD with Med15 ABD1 has apparently low specificity and affinity and is not sufficient to efficiently activate transcription by itself (Brzovic et al., 2011; Herbig et al., 2010). Additionally, transcription of many genes requires multiple activators, and it is not clear how or why specific combinations of activators synergize. To investigate this long-standing question, we examined the binding of Gcn4 with the Mediator subunit Med15. Gcn4 has the common arrangement of tandem ADs whereas Med15 has multiple ABDs, typical of most coactivator complexes. Based on earlier findings, two models can explain the requirement for multiple ADs and ABDs in this system: (1) expansion of the cAD-ABD1 fuzzy binding mechanism to encompass dynamic fuzzy interfaces between the two ADs and all ABDs or (2) a mechanism where the final complex adopts a discrete state due to stable binding and specific AD-ABD interactions. The latter model has been observed in two systems involving IDP binding to structured proteins that contain multiple binding sites (Dyson and Wright, 2016; Saio et al., 2014), whereas the former model has yet to be observed experimentally. The distinctions between these models have important implications for the flexibility of AD-ABD combinations used in activation of specific genes and in regulatory circuits where activators can combine to give complex patterns of gene regulation. For example, the locked down mechanism requires pairing ADs

and ABDs in specific combinations, as only particular pairings are expected to work together. At the other extreme, activators like Gcn4, Gal4, VP16, and p53 interact with many unrelated coactivators. Use of one or the other mechanisms demands a tradeoff between specificity of interactions and flexibility in regulation of a wide variety of genes with different coactivator requirements.

Our results demonstrate unambiguously that Gcn4-Med15 binding uses a fuzzy free-for-all mechanism, where each AD interacts with all ABDs. NMR CSP and backbone dynamics data show that the primary interacting regions of tAD are residues 94–98 and 120–124, but that the other hydrophobic regions are also directly involved in binding to Med15 ABDs, as supported by transcription activity assays. Protein crosslinking results show that Gcn4-Med15 is a heterogeneous complex, and binding measurements show that each Gcn4 AD can bind individual ABD1, 2, and 3 domains with micromolar affinity. Importantly, crosslinking experiments showed that multiple AD-ABD and AD-KIX binding interactions occur in the complex of full-length Gcn4 and Med15. Binding to KIX in the large complex is especially remarkable, as Gcn4-KIX binding is undetectable when separated from the rest of Med15. Surprisingly, crosslinks between Gcn4 and ABD3 are less frequent than with other ABDs, despite ABD3 having relatively high intrinsic affinity for both the nAD and cAD. Whereas it is possible that ABD3 does not efficiently bind Gcn4 in the large Gcn4-Med15 complex, we think it likely that binding occurs but that fewer crosslinks are detected for technical reasons. Crosslinking efficiency and/or detection of crosslinked products can be affected if crosslinkable residues are not in close proximity or if crosslinked peptides are not well detected by mass spectrometry (MS). The fact that ABD3 is as functionally important for Gcn4 activation as KIX, ABD1, and ABD2 (Herbig et al., 2010), combined with relatively strong Gcn4-ABD3 binding (Table 1), makes a strong case that this interaction does occur in the context of the larger complex. Also consistent with the fuzzy binding mechanism, our NMR results show that both ADs of Gcn4 bind Med15 independently within the large Gcn4-Med15 complex. Importantly, ABD1 and ABD2 have highly similar NMR CSPs, regardless of which AD variant is binding. Such behavior is not consistent with a specific binding interface and is again in agreement with the fuzzy binding model where the ABDs seem to recognize a cloud of hydrophobicity rather than a specific sequence. Finally, multiple spin-label probes positioned on the tAD showed unequivocally that tAD binds in multiple orientations on both ABD1 and ABD2.

Med15 is a subunit of the Mediator tail module (Med2, 3, 5, 15, and 16), and whether activator-Med15 binding has a role in the architecture and function of the tail is not yet clear. There is contradictory information on the function and relationship of these subunits in tail module function. In some reports, the function of several tail subunits seems redundant, whereas, in others, these subunits make equal and important contributions to transcription activation (Ansari et al., 2012; Ansari and Morse, 2012; Zhang et al., 2004). It is possible that Gcn4-Med15 binding causes a conformational change in tail or leads to other changes in the Mediator head or middle modules that affect function. However, in recent cryoelectron microscopy (cryo-EM) structures of yeast Mediator with and without other PIC components, the Med15-containing tail module remains disordered even when Gcn4 is present (Nozawa et al., 2017; Robinson et al., 2015; Tsai et al., 2017). This is consistent with our findings that Med15 contains multiple well-ordered activator binding domains separated by long flexible

linkers and that interactions of Gcn4 with each ABD do not result in a well-ordered complex. In agreement with these results, crosslinking of the Gcn4 ADs within the PIC is almost exclusive to Med15, whereas Med2, 3, 5, and 16 form a network of interactions that primarily crosslink with the Med15 C-terminal half that lies outside of the activator-binding region (Robinson et al., 2016). A crosslink between Gcn4 and Med16 was observed at a low frequency, but it is not known whether these polypeptides interact directly.

Whereas activator-Med15 binding naturally occurs in the larger context of the complete Mediator complex, it seems likely that the fuzzy interfaces described here will exist in this larger complex. The simple nature of the binding interfaces on ABD1 and ABD2 and the variety of AD sequences that bind seem to preclude precise molecular complementarity. Given the sequence variability of the ADs studied here and our previous findings that even more strongly binding synthetic ADs bind with a fuzzy interface (Warfield et al., 2014), we expect that fuzzy binding is a general feature of many large AD-Med15 complexes. Furthermore, the Med15 ABDs may be representative of protein domains designed to accommodate fuzzy interactions.

Whereas both ABD1 and ABD2 bind Gcn4 with a fuzzy interface, each uses a different type of surface feature to bind ADs. ABD1 has a shallow hydrophobic groove that can accommodate a variety of hydrophobic sequences in different orientations (Brzovic et al., 2011; Warfield et al., 2014), whereas ABD2 uses two separate hydrophobic surface patches. It is hard to imagine that individual AD-ABD interactions are specific enough for a biological response. However, the combination of ADs and multiple ABDs within Mediator gives rise to binding specificity, higher affinity, and function and allows important contributions to be made by very weak protein-protein interactions (e.g., Gcn4-KIX and cAD-ABD2; Figure 6). This combinatorial mechanism likely explains why most coactivator complexes examined to date (e.g., Mediator, Swi/Snf, and NuA4/SAGA) have multiple ABDs. Even though not every activator has multiple ADs, many ADs bind DNA as dimers, and a common regulatory strategy is to require combinations of transcription factors to bind to regulatory regions for efficient activation of transcription. We imagine that this mechanism has the same effect as multiple ADs in a single factor. It has been proposed that the fuzzy binding mechanism leads to higher affinity binding, in part by decreasing the dissociation rate due to multiple independent binding sites on both binding partners (Olsen et al., 2017).

In the broader context, it is important to note that not all activators work by this mechanism. There are several instances of ADs that bind their targets using specific protein-protein interfaces with much higher affinity. An intermediate case is that of ETV4 and Med25. On its own, the ETV4 DNA-binding domain (DBD) binds multiple sites on Med25, including the primary ETV4 AD binding site. When both ETV4 AD and DBD are present, a tighter binding complex is formed in which the AD binds one site, whereas the DBD may retain a fuzzy interface involving two other Med25 binding surfaces (Currie et al., 2017). Alternatively, the mammalian coactivator CBP contains numerous activator-binding domains whose individual ABDs partner with specific transcription activators using high-affinity conventional protein-protein interfaces (Dames et al., 2002; Demarest et al., 2002; Freedman et al., 2002; Radhakrishnan et al., 1997; Waters et al., 2006; Zor et al., 2004). We believe

that the fuzzy binding mode identified for Gcn4-Med15 is another common regulatory strategy and can account for the behavior in instances where ADs are known to interact with multiple unrelated coactivators. This strategy can generate great flexibility in developing new regulatory circuits where many combinations of activators can regulate a wide variety of genes with different coactivator requirements. It seems likely that a similar strategy will be utilized in other biological systems that utilize IDPs reacting with multiple partners.

EXPERIMENTAL PROCEDURES

Further details and an outline of resources used in this work can be found in Supplemental Experimental Procedures.

Contact for Reagent and Resource Sharing

Further information and requests for resources and reagents should be directed to and will be fulfilled by the corresponding authors, Steve Hahn (shahn@fredhutch.org) or Rachel Klevit (klevit@u.washington.edu).

Yeast Strains and Plasmids

Yeast strain SHY823 (Δ*gcn4, leu2*) was transformed with the following *LEU2* and GCN4-derivative plasmids for protein expression and mRNA analysis: pRS315 (vector—no *GCN4*), pSH940 (WT *GCN4*), and pSH943 (Gcn4 Δ101–124; [nAD] with the flexible linker: GSGSGS at the junction of the internal deletion) (Herbig et al., 2010). Gcn4 nAD mutations were generated in pSH943 by site-directed mutagenesis. All Gcn4 derivatives contained a C-terminal 3X-FLAG tag.

mRNA Analysis

RNA was extracted and assayed in triplicate by qRT-PCR, and the results were analyzed as described (Herbig et al., 2010).

Protein Purification

All proteins were expressed in BL21 (DE3) RIL *E. coli*. Med15 484–651 (ABD3), Med15 158–651 Δ239–272, Δ373–483 (ABD123), and Med15 1–651 Δ239–272, Δ373–483 (KIX123) were expressed as N-terminal His6-tagged proteins. All other Med15 and Gcn4 constructs were expressed as N-terminal His6-SUMO-tagged proteins. Cells were lysed in 50 mM HEPES (pH 7.0), 500 mM NaCl, 40 mM imidazole, 10% glycerol, 1 mM PMSF, 5 mM DTT and purified using Ni-Sepharose High Performance resin (GE Healthcare). Proteins were eluted in 50 mM HEPES (pH 7.0), 500 mM NaCl, 500 mM imidazole, 10% glycerol, 1 mM PMSF, 1 mM DTT. Purified SUMO-tagged proteins were concentrated using 10K MW cutoff centrifugal filters (Millipore), diluted 10× in 50 mM HEPES (pH 7.0), 500 mM NaCl, 40 mM imidazole, 10% glycerol, 1 mM PMSF, 5 mM DTT, and digested with SUMO protease for 3–5 hr at room temperature using ~1:800 protease: protein ratio. Cleaved His6-Sumo tag was removed using Ni-Sepharose. Med15 polypeptides were further purified using HiTrap Heparin (GE Healthcare) in 20 mM HEPES (pH 7), 1 mM DTT, 0.5 mM PMSF eluting with either a 50–350 mM NaCl gradient (ABD1 and ABD2) or a 200–600 mM NaCl gradient (ABD3, ABD123, and KIX123). Gcn4 AD derivatives 1–134 and

101–134 were further purified by chromatography on Source 15Q (GE Healthcare) using a 50–350 mM NaCl gradient. Gcn4 1–100 and other nAD derivatives were purified using Source 15Q and HiTrap Phenyl FF (GE Healthcare). Protein was loaded to Source 15Q at 120 mM NaCl and flowed through the column. This unbound fraction was adjusted to 0.8 M $(NH_4)_2SO_4$, bound to phenyl FF, and eluted with an 800–0 mM $(NH_4)_2SO_4$ gradient. All proteins were further purified using size exclusion chromatography on Superdex 75 10/30 (GE Healthcare). Proteins used in fluorescence polarization and isothermal titration calorimetry were eluted in 20 mM KH_2PO_4 (pH 7.5), 200 mM KCl. Proteins used in cross-linking-MS were eluted in PBS (pH 7.2). Proteins used in NMR were eluted in 20 mM NaH_2PO_4 (pH 6.5), 200 mM NaCl, 0.1 mM EDTA, 0.1 mM PMSF, 5 mM DTT. The concentration of the purified proteins was determined by UV-Vis (ultraviolet-visible) spectroscopy with extinction coefficients calculated with ProtParam (Gasteiger et al., 2005).

FP and ITC Binding Experiments

Gcn4 peptides used in fluorescence polarization were labeled with Oregon Green 488 dye (Invitrogen) as previously described (Herbig et al., 2010). FP measurements were conducted using a Beacon 2000 instrument as previously described (Herbig et al., 2010). Protein concentrations for titrations with Gcn4 nAD and Gcn4 cAD were as described (Herbig et al., 2010), except for Gcn4 cAD versus Med15 ABD3 (0–225 μM). Titrations between Gcn4 tAD and Med15 were performed with 15 concentrations of Med15 spanning 0–135 μM (KIX) or 0–250 μM (ABD1, ABD2, ABD3, ABD123, and KIX123). FP data were analyzed using Prism 7 (Graphpad Software) to perform non-linear regression analysis using the one-site total binding model $Y = B_{max}*X/(K_d + X) + NS*X + Background$, where Y equals arbitrary polarization units and X equals Med15 concentration.

Isothermal calorimetry titrations were performed using a Microcal ITC200 Microcalorimeter in 20 mM KH_2PO_4 (pH 7.5), 200 mM KCl as described in (Brzovic et al., 2011). The following protein concentrations were used, with the cell molecule listed first and the syringe molecule listed second: Med15 ABD1 (0.150 mM) versus Gcn4 nAD (1.50 mM); Gcn4 nAD (0.111 mM) versus Med15 ABD2 (1.60 mM); Gcn4 nAD (0.111 mM) versus Med15 ABD3 (1.12 mM); Med15 ABD1 (0.270 mM) versus Gcn4 cAD (2.37 mM); Med15 ABD2 (0.224 mM) versus Gcn4 cAD (2.35 mM); and Med15 ABD3 (0.236 mM) versus Gcn4 cAD (2.35 mM). Calorimetric data were plotted and fit with a single binding site model using Origin 7.0 software (Microcal). Some affinities could not be measured by ITC, either due to weak binding or low heats of binding.

Protein Crosslinking and Sample Preparation for Mass Spectrometry

50 μg of Med15 158–651 Δ239–272, Δ373–483 (ABD123) or Med15 1–651 Δ239–272, Δ373–483 (KIX123) was mixed with 3x molar excess of Gcn4 1–140. Samples were incubated with 5 mM (for ABD123 experiments) or 7.5 mM (for KIX123 experiments) EDC (1-ethyl-3-(3-dimethylaminopropyl)carbodiimide hydrochloride; Thermo Scientific), and 2 mM Sulfo-NHS (Thermo Scientific) in 100 μL total volume for 2 hr at room temperature. Protein samples were reduced with 50 mM TCEP and denatured with 8 M urea at 37°C for 15 min. The samples were then alkylated in the dark at 37°C with 15 mM iodoacetamide for 1 hr. The samples were then diluted 10-fold with 100 mM ammonium bicarbonate and

digested with trypsin (1:15 w/w) overnight at 37°C. Digested samples were purified by C18 chromatography (Waters), eluted in 80% acetonitrile 0.15 trifluoroacetic acid, and dried in a SpeedVac.

Mass Spectrometry for Identification of Crosslinks

Peptides were analyzed using a Thermo Scientific Orbitrap Elite with HCD fragmentation and serial MS events that included one FTMS1 event at 15,000 resolution followed by 10 FTMS2 events at 7,500 resolution. Other instrument settings included the following: charge state rejection: +1, +2, +3, and unassigned charges; monoisotopic precursor selection enabled; dynamic exclusion enabled: repeat count 1, exclusion list size 500, exclusion duration 30 s; HCD normalized collision energy 35%, isolation width 3 Da, minimum signal count 5,000; MS mass range: >1,500, use m/z values as masses enabled; and FTMS MSn AGC target 500,000, FTMS MSn Max ion time 300 ms. Peptides were resolved by online reverse phase HPLC (high-performance liquid chromatography) using a 90 min gradient from 5% ACN to 40% ACN.

To identify EDC-crosslinked peptides, two different database search algorithms were used: pLink (Yang et al., 2012) and in-house-designed Nexus (Luo et al., 2015). pLink was run with default settings (precursor monoisotopic mass tolerance: ±10 ppm; fragment mass tolerance: ±20 ppm; up to 4 isotopic peaks; max evalue 0.1; static modification on cysteines; 57.0215 Da; differential oxidation modification on methionines; 15.9949 Da) using a database containing the target protein sequences. For Nexus searches, a protein database containing the forward and reversed sequences of the target proteins was used with the following parameter settings: up to three miscleavages; static modification on cysteines (+57.0215 Da); differential oxidation modification on methionines (+15.9949 Da); and differential modification on the peptide N-terminal glutamic acid residues (−18.0106 Da) or N-terminal glutamine residues (−17.0265 Da). GluC and trypsin were specified as the digestion enzymes, and a 5% FDR (false discovery rate) was used for both searches. After performing the pLink and the Nexus analyses, the search results were combined, and each spectrum was manually evaluated for the quality of the match to each peptide using the COMET/Lorikeet Spectrum Viewer (TPP). A crosslinked peptide was considered to be confidently identified if at least four consecutive b or y ions for each peptide was observed and the majority of the observed ions were accounted for.

NMR Experiments and Resonance Assignments

NMR HSQC titration, dynamics, and spin-label experiments were completed on a Bruker 500 MHz AVANCE spectrometer. All spectra were collected at 25°C in NMR buffer (20 mM sodium phosphate, 150 mM NaCl, 0.1 mM EDTA, 0.1 mM PMSF, and 5 mM DTT) with 7% D_2O, unless otherwise specified. Spin-label samples were in NMR buffer but with no DTT; dynamics and titration samples were in NMR buffer but with 200 mM NaCl because ABD3 is more stable at higher salt.

(^{1}H,^{15}N)- and (^{1}H,^{13}C)-HSQC titration experiments were completed for all Gcn4-AD:Med15-ABD combinations by adding unlabeled AD (nAD, cAD, tAD) or ABD (ABD1, ABD2, ABD3, ABD123) to a ~200 μM [^{13}C,^{15}N]-AD or ABD sample, maintaining a

constant concentration of the labeled species. T_1 and T_2 ^{15}N-Trosy HSQC experiments for 200 μM [^{13}C,^{15}N]-nAD and 200 μM [^{13}C,^{15}N]-nAD + 600 μM ABD1 were collected in an interleaved manner with 8 points each (Zhu et al., 2000). T_1 delays were 10, 40, 80, 120, 160, 320, 640, and 1,000 ms; T_2 cpmg loop delays were 8.48, 16.96, 25.44, 33.92, 42.40, 50.88, 59.36, and 67.84 ms. T_1 and T_2 for each residue were fitted to a single exponential with errors reflecting the quality in the fit.

Paramagnetic relaxation enhancement (PRE) experiments were performed as for cAD:ABD1 (Brzovic et al., 2011) but at lower saturation. The spin-label 4-(2-iodoacetamido)-TEMPO was incorporated at T82C (nAD and tAD), T105C (tAD), and S117C (cAD and tAD) by incubating the AD Cys mutants with 10x TEMPO overnight at room temperature, followed by several hours at 30°C. Excess TEMPO was removed by elution over a Nap-10 column and buffer exchange during concentration. ^{15}N- and ^{13}C-HSQC spectra of [^{13}C,^{15}N]-ABD1 and [^{13}C,^{15}N]-ABD2 with spin-labeled ADs at a ~2:1 ABD:AD concentration ratio were collected in the presence (reference intensity, I_{dia}) and absence of 3 mM ascorbic acid (I_{para}). A control sample was collected of [^{13}C,^{15}N]-ABD2 with 500 μM free TEMPO, with and without 3 mM ascorbic acid.

Gcn4 tAD (aa 1–134) chemical shift assignments were transferred from nAD (aa 1–100) and cAD (aa 101–134) assignments (Brzovic et al., 2011) where possible and verified by standard backbone triple-resonance experiments (HNCA, HNCOCA, HNCOCACB, HNCACB, and HNCO) obtained on a 400 μM [^{13}C,^{15}N]-tAD sample using Bruker 500 and 600 MHz Avance spectrometers. Gcn4 nAD chemical shift assignments were transferred from mini-nAD (Gcn4 1–100, Δ21–40, 52–60) where possible and verified by standard backbone triple-resonance experiments obtained on a 350 μM [^{13}C,^{15}N]-nAD + 620 μM ABD1 sample using Bruker 500 and 600 MHz Avance spectrometers. Assignments of free nAD were determined by following HSQC titration trajectories of nAD + ABD1. Mini-nAD assignments were obtained on a 600 μM [^{13}C,^{15}N]-mini-nAD sample using standard experiments on a Varian INOVA 600 or 800 MHz instruments located at Pacific Northwest National Laboratories.

Med15 ABD2 (residues 277–368) backbone and side-chain chemical shift assignments were obtained on ~1 mM [^{13}C,^{15}N]-ABD2 using standard experiments (HNCA, HNCOCA, HNCACB, HNCO, ^{15}N-TOCSY, ^{15}N-NOESY, aromatic and aliphatic ^{13}C-NOESY, HNHAHB, HCCONH, CCONH, HCCH-TOCSY, and HCCH-COSY) on Bruker 600 and 800 MHz Avance spectrometers. ^{13}C-NOESY and HCCH experiments were collected in D_2O NMR buffer. HSQC and NOESY experiments were also collected on a [^{13}C,^{15}N]-F319Y ABD2 mutant sample to assist in assignments of aromatic residues and NOEs (Figure S4A). (^{1}H,^{15}N)-HSQC-IPAP experiments for measuring D_{NH} RDCs were collected on a ^{15}N-ABD2 sample at 22°C using a C12E6/hexanol mixture for alignment (Higman et al., 2011) on a Bruker 800 MHz Avance spectrometer.

The NH chemical shift perturbation was calculated according to $\Delta\delta_{NH}$ (ppm) = sqrt [$\Delta\delta_H^2$ + ($\Delta\delta_N$/5)^2]. Component ^{1}H and ^{15}N CSPs are (freeform—bound form) in ppm. Secondary structure propensity was determined from backbone chemical shifts using the Neighbor-Corrected Structural Propensity Calculator (ncSPC) (Tamiola and Mulder, 2012). Max CSP

as in Figure S3B represents the maximum CSP of any residue within each defined hydrophobic cluster.

NMR Solution Structure

The structure of freeform Med15 ABD2 (aa 277–368) was determined based on chemical shifts, NOEs, and N-H RDCs using the Xplor-NIH software (Schwieters et al., 2003) with the EEFx implicit water potential (Tian et al., 2014). NOEs were assigned manually and used as distance restraints. Dihedral backbone restraints were calculated from backbone chemical shifts using TALOS (Shen and Bax, 2013) and were only used for residues with "strong" database matches. Structure calculations were based on the recommended eefx/fold.py and refine.py scripts, which are included with the software. Simulations start from an extended conformation of ABD2, followed by rounds of simulated annealing and cooling to find the 20 lowest energy of 200 generated structures. Structure validation and statistics (Table S3) were determined using the Protein Structure Validation Software (PSVS) web server (Basu et al., 2008) and Procheck via the wwPDB submission (Berman et al., 2003). Electrostatic surfaces were generated using PDB2QPR and the APBS tool in pymol (Dolinsky et al., 2004).

Quantification and Statistical Analyses

mRNA Quantification—Steady-state mRNA levels were quantitated by qRT-PCR as described above and in Herbig et al. (2010).

Mass Spectrometry and Data Analysis—EDC-crosslinked peptides were analyzed on a Thermo Scientific Orbitrap Elite at the Proteomics facility at the Fred Hutchinson Cancer Research Center, and data were analyzed as described (Knutson et al., 2014). Two different database search algorithms were used to identify EDC-crosslinked peptides: pLink (Yang et al., 2012) and the in-house-designed Nexus (Luo et al., 2015). A 5% FDR was used for the results from both searches. Spectra were manually evaluated using the COMET/Lorikeet Spectrum Viewer (Trans-Proteomic Pipeline) (Knutson et al., 2014).

NMR Analysis—All NMR spectra were processed using NMRPipe (Delaglio et al., 1995) and analyzed in nmrViewJ (Johnson, 2004). NMR peak intensities for spin-label experiments were quantified using NMRviewJ, and error bars reflect noise levels of the spectra. Peak centers for RDC measurements were determined using FuDA (Hansen et al., 2007). Percent saturation was calculated based on the K_d for each A:B complex according to $\%sat = [AB]/A = (1/A)*(C/2 + (C^2 – 4*A*B)^{0.5})$, where $A = [A_{total}]$, $B = [B_{total}]$, and $C = A + B + K_d$.

DATA AND SOFTWARE AVAILABILITY

The solution structure of Med15 ABD2 has been deposited in the Protein Data Bank with the accession code PDB: 6ALY. NMR chemical shifts, NOEs, and RDCs have been deposited to the BioMagResBank with the accession numbers BioMagResBank: 30330 for ABD2 and BioMagResBank: 27207 for Gcn4 tAD 1–134. NMR and crosslinking data have been deposited in the Mendeley Data repository (https://doi.org/10.17632/twjfm5rnnm.1).

Supplementary Material

Refer to Web version on PubMed Central for supplementary material.

Acknowledgments

We thank Ponni Rajagopal and Peter Brzovic of the Klevit laboratory for collection of some of the NMR data, Alexia Loste (Univ Paris, Diderot) for Med15 and Gcn4 expression constructs and for initial crosslinking studies of Gcn4-Med15, and all members of the Klevit and Hahn laboratories for their suggestions and comments during this work. This work was facilitated by the use of advanced computational infrastructure provided by the Hyak supercomputer system at the University of Washington. NMR experiments were performed, in part, in the Environmental Molecular Sciences Laboratories at the Pacific Northwest National Laboratories. This work was funded by NIH RO1 GM075114 to S.H. and R.E.K. and RO1 GM110064 and P50 GM076547 to J.R.

References

Ansari SA, Morse RH. Selective role of Mediator tail module in the transcription of highly regulated genes in yeast. Transcription. 2012; 3:110–114. [PubMed: 22771944]

Ansari SA, Ganapathi M, Benschop JJ, Holstege FC, Wade JT, Morse RH. Distinct role of Mediator tail module in regulation of SAGA-dependent, TATA-containing genes in yeast. EMBO J. 2012; 31:44–57. [PubMed: 21971086]

Basu A, Samanta D, Bhattacharya A, Das A, Das D, Dasgupta C. Protein folding following synthesis in vitro and in vivo: association of newly synthesized protein with 50S subunit of E. coli ribosome. Biochem Biophys Res Commun. 2008; 366:592–597. [PubMed: 18062922]

Berman H, Henrick K, Nakamura H. Announcing the worldwide Protein Data Bank. Nat Struct Biol. 2003; 10:980. [PubMed: 14634627]

Brown CE, Howe L, Sousa K, Alley SC, Carrozza MJ, Tan S, Workman JL. Recruitment of HAT complexes by direct activator interactions with the ATM-related Tra1 subunit. Science. 2001a; 292:2333–2337. [PubMed: 11423663]

Brown DR, Deb D, Frum R, Hickes L, Munoz R, Deb S, Deb SP. The human oncoprotein MDM2 uses distinct strategies to inhibit transcriptional activation mediated by the wild-type p53 and its tumor-derived mutants. Int J Oncol. 2001b; 18:449–459. [PubMed: 11179471]

Brzovic PS, Heikaus CC, Kisselev L, Vernon R, Herbig E, Pacheco D, Warfield L, Littlefield P, Baker D, Klevit RE, Hahn S. The acidic transcription activator Gcn4 binds the mediator subunit Gal11/Med15 using a simple protein interface forming a fuzzy complex. Mol Cell. 2011; 44:942–953. [PubMed: 22195967]

Chang J, Kim DH, Lee SW, Choi KY, Sung YC. Transactivation ability of p53 transcriptional activation domain is directly related to the binding affinity to TATA-binding protein. J Biol Chem. 1995; 270:25014–25019. [PubMed: 7559631]

Currie SL, Doane JJ, Evans KS, Bhachech N, Madison BJ, Lau DKW, McIntosh LP, Skalicky JJ, Clark KA, Graves BJ. ETV4 and AP1 transcription factors form multivalent interactions with three sites on the MED25 activator-interacting domain. J Mol Biol. 2017; 429:2975–2995. [PubMed: 28728983]

Dames SA, Martinez-Yamout M, De Guzman RN, Dyson HJ, Wright PE. Structural basis for Hif-1 alpha /CBP recognition in the cellular hypoxic response. Proc Natl Acad Sci USA. 2002; 99:5271–5276. [PubMed: 11959977]

Delaforge E, Kragelj J, Tengo L, Palencia A, Milles S, Bouvignies G, Salvi N, Blackledge M, Jensen MR. Deciphering the dynamic interaction profile of an intrinsically disordered protein by NMR exchange spectroscopy. J Am Chem Soc. 2018; 140:1148–1158. [PubMed: 29276882]

Delaglio F, Grzesiek S, Vuister GW, Zhu G, Pfeifer J, Bax A. NMRPipe: a multidimensional spectral processing system based on UNIX pipes. J Biomol NMR. 1995; 6:277–293. [PubMed: 8520220]

Demarest SJ, Martinez-Yamout M, Chung J, Chen H, Xu W, Dyson HJ, Evans RM, Wright PE. Mutual synergistic folding in recruitment of CBP/p300 by p160 nuclear receptor coactivators. Nature. 2002; 415:549–553. [PubMed: 11823864]

Díaz-Santín LM, Lukoyanova N, Aciyan E, Cheung AC. Cryo-EM structure of the SAGA and NuA4 coactivator subunit Tra1 at 3.7 angstrom resolution. eLife. 2017; 6:e28384. [PubMed: 28767037]

Dolinsky TJ, Nielsen JE, McCammon JA, Baker NA. PDB2PQR: an automated pipeline for the setup of Poisson-Boltzmann electrostatics calculations. Nucleic Acids Res. 2004; 32:W665–W667. [PubMed: 15215472]

Drysdale CM, Dueñas E, Jackson BM, Reusser U, Braus GH, Hinnebusch AG. The transcriptional activator GCN4 contains multiple activation domains that are critically dependent on hydrophobic amino acids. Mol Cell Biol. 1995; 15:1220–1233. [PubMed: 7862116]

Dyson HJ, Wright PE. Intrinsically unstructured proteins and their functions. Nat Rev Mol Cell Biol. 2005; 6:197–208. [PubMed: 15738986]

Dyson HJ, Wright PE. Role of intrinsic protein disorder in the function and interactions of the transcriptional coactivators CREB-binding protein (CBP) and p300. J Biol Chem. 2016; 291:6714–6722. [PubMed: 26851278]

Ferreira ME, Prochasson P, Berndt KD, Workman JL, Wright AP. Activator-binding domains of the SWI/SNF chromatin remodeling complex characterized in vitro are required for its recruitment to promoters in vivo. FEBS J. 2009; 276:2557–2565. [PubMed: 19476494]

Ferreon JC, Lee CW, Arai M, Martinez-Yamout MA, Dyson HJ, Wright PE. Cooperative regulation of p53 by modulation of ternary complex formation with CBP/p300 and HDM2. Proc Natl Acad Sci USA. 2009; 106:6591–6596. [PubMed: 19357310]

Fishburn J, Mohibullah N, Hahn S. Function of a eukaryotic transcription activator during the transcription cycle. Mol Cell. 2005; 18:369–378. [PubMed: 15866178]

Freedman SJ, Sun ZY, Poy F, Kung AL, Livingston DM, Wagner G, Eck MJ. Structural basis for recruitment of CBP/p300 by hypoxia-inducible factor-1 alpha. Proc Natl Acad Sci USA. 2002; 99:5367–5372. [PubMed: 11959990]

Gasteiger, E., Hoogland, C., Gattiker, A., Duvaud, S., Wilkins, MR., Appel, RD., Bairoch, A. Protein identification and analysis tools on the ExPASy server. In: Walker, JM., editor. The Proteomics Protocols Handbook. Humana Press; 2005. p. 571-607.

Hahn S, Young ET. Transcriptional regulation in Saccharomyces cerevisiae: transcription factor regulation and function, mechanisms of initiation, and roles of activators and coactivators. Genetics. 2011; 189:705–736. [PubMed: 22084422]

Hansen DF, Yang D, Feng H, Zhou Z, Wiesner S, Bai Y, Kay LE. An exchange-free measure of 15N transverse relaxation: an NMR spectroscopy application to the study of a folding intermediate with pervasive chemical exchange. J Am Chem Soc. 2007; 129:11468–11479. [PubMed: 17722922]

Herbig E, Warfield L, Fish L, Fishburn J, Knutson BA, Moorefield B, Pacheco D, Hahn S. Mechanism of Mediator recruitment by tandem Gcn4 activation domains and three Gal11 activator-binding domains. Mol Cell Biol. 2010; 30:2376–2390. [PubMed: 20308326]

Higman VA, Boyd J, Smith LJ, Redfield C. Residual dipolar couplings: are multiple independent alignments always possible? J Biomol NMR. 2011; 49:53–60. [PubMed: 21184138]

Jackson BM, Drysdale CM, Natarajan K, Hinnebusch AG. Identification of seven hydrophobic clusters in GCN4 making redundant contributions to transcriptional activation. Mol Cell Biol. 1996; 16:5557–5571. [PubMed: 8816468]

Jedidi I, Zhang F, Qiu H, Stahl SJ, Palmer I, Kaufman JD, Nadaud PS, Mukherjee S, Wingfield PT, Jaroniec CP, Hinnebusch AG. Activator Gcn4 employs multiple segments of Med15/Gal11, including the KIX domain, to recruit mediator to target genes in vivo. J Biol Chem. 2010; 285:2438–2455. [PubMed: 19940160]

Johnson BA. Using NMRView to visualize and analyze the NMR spectra of macromolecules. Methods Mol Biol. 2004; 278:313–352. [PubMed: 15318002]

Knutson BA, Hahn S. Domains of Tra1 important for activator recruitment and transcription coactivator functions of SAGA and NuA4 complexes. Mol Cell Biol. 2011; 31:818–831. [PubMed: 21149579]

Knutson BA, Luo J, Ranish J, Hahn S. Architecture of the Saccharomyces cerevisiae RNA polymerase I core factor complex. Nat Struct Mol Biol. 2014; 21:810–816. [PubMed: 25132180]

Langlois C, Mas C, Di Lello P, Jenkins LM, Legault P, Omichinski JG. NMR structure of the complex between the Tfb1 subunit of TFIIH and the activation domain of VP16: structural similarities between VP16 and p53. J Am Chem Soc. 2008; 130:10596–10604. [PubMed: 18630911]

Levine M, Cattoglio C, Tjian R. Looping back to leap forward: transcription enters a new era. Cell. 2014; 157:13–25. [PubMed: 24679523]

Luo J, Cimermancic P, Viswanath S, Ebmeier CC, Kim B, Dehecq M, Raman V, Greenberg CH, Pellarin R, Sali A, et al. Architecture of the human and yeast general transcription and DNA repair factor TFIIH. Mol Cell. 2015; 59:794–806. [PubMed: 26340423]

Natarajan K, Meyer MR, Jackson BM, Slade D, Roberts C, Hinnebusch AG, Marton MJ. Transcriptional profiling shows that Gcn4p is a master regulator of gene expression during amino acid starvation in yeast. Mol Cell Biol. 2001; 21:4347–4368. [PubMed: 11390663]

Nguyen Ba AN, Yeh BJ, van Dyk D, Davidson AR, Andrews BJ, Weiss EL, Moses AM. Proteome-wide discovery of evolutionary conserved sequences in disordered regions. Sci Signal. 2012; 5:rs1. [PubMed: 22416277]

Novatchkova M, Eisenhaber F. Linking transcriptional mediators via the GACKIX domain super family. Curr Biol. 2004; 14:R54–R55. [PubMed: 14738747]

Nozawa K, Schneider TR, Cramer P. Core Mediator structure at 3.4 Å extends model of transcription initiation complex. Nature. 2017; 545:248–251. [PubMed: 28467824]

Olsen JG, Teilum K, Kragelund BB. Behaviour of intrinsically disordered proteins in protein-protein complexes with an emphasis on fuzziness. Cell Mol Life Sci. 2017; 74:3175–3183. [PubMed: 28597296]

Prochasson P, Neely KE, Hassan AH, Li B, Workman JL. Targeting activity is required for SWI/SNF function in vivo and is accomplished through two partially redundant activator-interaction domains. Mol Cell. 2003; 12:983–990. [PubMed: 14580348]

Prochasson P, Florens L, Swanson SK, Washburn MP, Workman JL. The HIR corepressor complex binds to nucleosomes generating a distinct protein/DNA complex resistant to remodeling by SWI/SNF. Genes Dev. 2005; 19:2534–2539. [PubMed: 16264190]

Qiu H, Chereji RV, Hu C, Cole HA, Rawal Y, Clark DJ, Hinnebusch AG. Genome-wide cooperation by HAT Gcn5, remodeler SWI/SNF, and chaperone Ydj1 in promoter nucleosome eviction and transcriptional activation. Genome Res. 2016; 26:211–225. [PubMed: 26602697]

Radhakrishnan I, Pérez-Alvarado GC, Parker D, Dyson HJ, Montminy MR, Wright PE. Solution structure of the KIX domain of CBP bound to the transactivation domain of CREB: a model for activator:coactivator interactions. Cell. 1997; 91:741–752. [PubMed: 9413984]

Regier JL, Shen F, Triezenberg SJ. Pattern of aromatic and hydrophobic amino acids critical for one of two subdomains of the VP16 transcriptional activator. Proc Natl Acad Sci USA. 1993; 90:883–887. [PubMed: 8381535]

Robinson PJ, Trnka MJ, Pellarin R, Greenberg CH, Bushnell DA, Davis R, Burlingame AL, Sali A, Kornberg RD. Molecular architecture of the yeast Mediator complex. eLife. 2015; 4:e08719. [PubMed: 26402457]

Robinson PJ, Trnka MJ, Bushnell DA, Davis RE, Mattei PJ, Burlingame AL, Kornberg RD. Structure of a complete mediator-RNA polymerase II pre-initiation complex. Cell. 2016; 166:1411–1422 e16. [PubMed: 27610567]

Saio T, Guan X, Rossi P, Economou A, Kalodimos CG. Structural basis for protein antiaggregation activity of the trigger factor chaperone. Science. 2014; 344:1250494. [PubMed: 24812405]

Schwieters CD, Kuszewski JJ, Tjandra N, Clore GM. The Xplor-NIH NMR molecular structure determination package. J Magn Reson. 2003; 160:65–73. [PubMed: 12565051]

Shen Y, Bax A. Protein backbone and sidechain torsion angles predicted from NMR chemical shifts using artificial neural networks. J Biomol NMR. 2013; 56:227–241. [PubMed: 23728592]

Sigler PB. Transcriptional activation. Acid blobs and negative noodles. Nature. 1988; 333:210–212. [PubMed: 3367995]

Spitz F, Furlong EE. Transcription factors: from enhancer binding to developmental control. Nat Rev Genet. 2012; 13:613–626. [PubMed: 22868264]

Swanson MJ, Qiu H, Sumibcay L, Krueger A, Kim SJ, Natarajan K, Yoon S, Hinnebusch AG. A multiplicity of coactivators is required by Gcn4p at individual promoters in vivo. Mol Cell Biol. 2003; 23:2800–2820. [PubMed: 12665580]

Tamiola K, Mulder FA. Using NMR chemical shifts to calculate the propensity for structural order and disorder in proteins. Biochem Soc Trans. 2012; 40:1014–1020. [PubMed: 22988857]

Tantos A, Han KH, Tompa P. Intrinsic disorder in cell signaling and gene transcription. Mol Cell Endocrinol. 2012; 348:457–465. [PubMed: 21782886]

Tian Y, Schwieters CD, Opella SJ, Marassi FM. A practical implicit solvent potential for NMR structure calculation. J Magn Reson. 2014; 243:54–64. [PubMed: 24747742]

Tompa P, Davey NE, Gibson TJ, Babu MM. A million peptide motifs for the molecular biologist. Mol Cell. 2014; 55:161–169. [PubMed: 25038412]

Tsai KL, Yu X, Gopalan S, Chao TC, Zhang Y, Florens L, Washburn MP, Murakami K, Conaway RC, Conaway JW, Asturias FJ. Mediator structure and rearrangements required for holoenzyme formation. Nature. 2017; 544:196–201. [PubMed: 28241144]

Unger T, Nau MM, Segal S, Minna JD. p53: a transdominant regulator of transcription whose function is ablated by mutations occurring in human cancer. EMBO J. 1992; 11:1383–1390. [PubMed: 1314165]

Walker S, Greaves R, O'Hare P. Transcriptional activation by the acidic domain of Vmw65 requires the integrity of the domain and involves additional determinants distinct from those necessary for TFIIB binding. Mol Cell Biol. 1993; 13:5233–5244. [PubMed: 8395001]

Warfield L, Tuttle LM, Pacheco D, Klevit RE, Hahn S. A sequence-specific transcription activator motif and powerful synthetic variants that bind Mediator using a fuzzy protein interface. Proc Natl Acad Sci USA. 2014; 111:E3506–E3513. [PubMed: 25122681]

Waters L, Yue B, Veverka V, Renshaw P, Bramham J, Matsuda S, Frenkiel T, Kelly G, Muskett F, Carr M, Heery DM. Structural diversity in p160/CREB-binding protein coactivator complexes. J Biol Chem. 2006; 281:14787–14795. [PubMed: 16540468]

Weake VM, Workman JL. Inducible gene expression: diverse regulatory mechanisms. Nat Rev Genet. 2010; 11:426–437. [PubMed: 20421872]

Yang F, Vought BW, Satterlee JS, Walker AK, Jim Sun ZY, Watts JL, DeBeaumont R, Saito RM, Hyberts SG, Yang S, et al. An ARC/Mediator subunit required for SREBP control of cholesterol and lipid homeostasis. Nature. 2006; 442:700–704. [PubMed: 16799563]

Yang B, Wu YJ, Zhu M, Fan SB, Lin J, Zhang K, Li S, Chi H, Li YX, Chen HF, et al. Identification of cross-linked peptides from complex samples. Nat Methods. 2012; 9:904–906. [PubMed: 22772728]

Yoon S, Qiu H, Swanson MJ, Hinnebusch AG. Recruitment of SWI/SNF by Gcn4p does not require Snf2p or Gcn5p but depends strongly on SWI/SNF integrity, SRB mediator, and SAGA. Mol Cell Biol. 2003; 23:8829–8845. [PubMed: 14612422]

Zhang F, Sumibcay L, Hinnebusch AG, Swanson MJ. A triad of subunits from the Gal11/tail domain of Srb mediator is an in vivo target of transcriptional activator Gcn4p. Mol Cell Biol. 2004; 24:6871–6886. [PubMed: 15254252]

Zhu G, Xia Y, Nicholson LK, Sze KH. Protein dynamics measurements by TROSY-based NMR experiments. J Magn Reson. 2000; 143:423–426. [PubMed: 10729271]

Zor T, De Guzman RN, Dyson HJ, Wright PE. Solution structure of the KIX domain of CBP bound to the transactivation domain of c-Myb. J Mol Biol. 2004; 337:521–534. [PubMed: 15019774]

Highlights

- Tandem ADs of Gcn4 interact with Med15 ABDs in a fuzzy “free-for-all” complex
- Weak AD-ABD interactions significantly contribute to transcription activation
- Solution structure of Med15 ABD2 is reported
- Med15 ABDs may be designed to accommodate fuzzy interactions

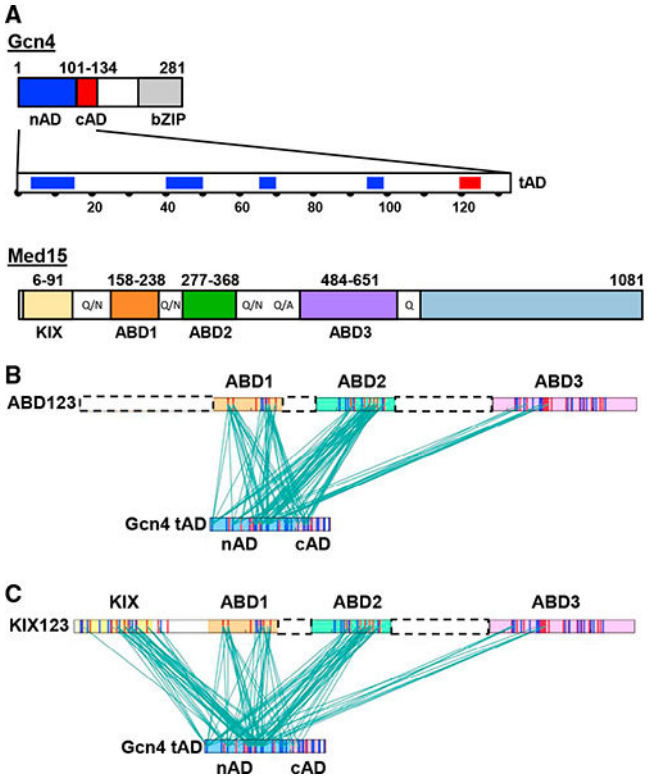

Figure 1. Gcn4 tAD Crosslinks to Each Med15 ABD and KIX

(A) Gcn4 consists of the tAD and bZIP subdomains. The expanded view of the tAD highlights key hydrophobic residue clusters located in the nAD (blue) and cAD (red). The four structured Med15 domains in the activator-binding region and the Q-rich linkers between the domains are indicated. (B and C) ABD123-tAD (B) and KIX123-tAD (C) crosslinking results. Lines between the Med15 and Gcn4 constructs indicate the sites of crosslinking that were identified by mass spectrometry. Dashed boxes indicate deleted regions of the wild-type sequence for each Med15 construct. Red and blue bars within each subdomain indicate acidic and lysine residues, respectively.

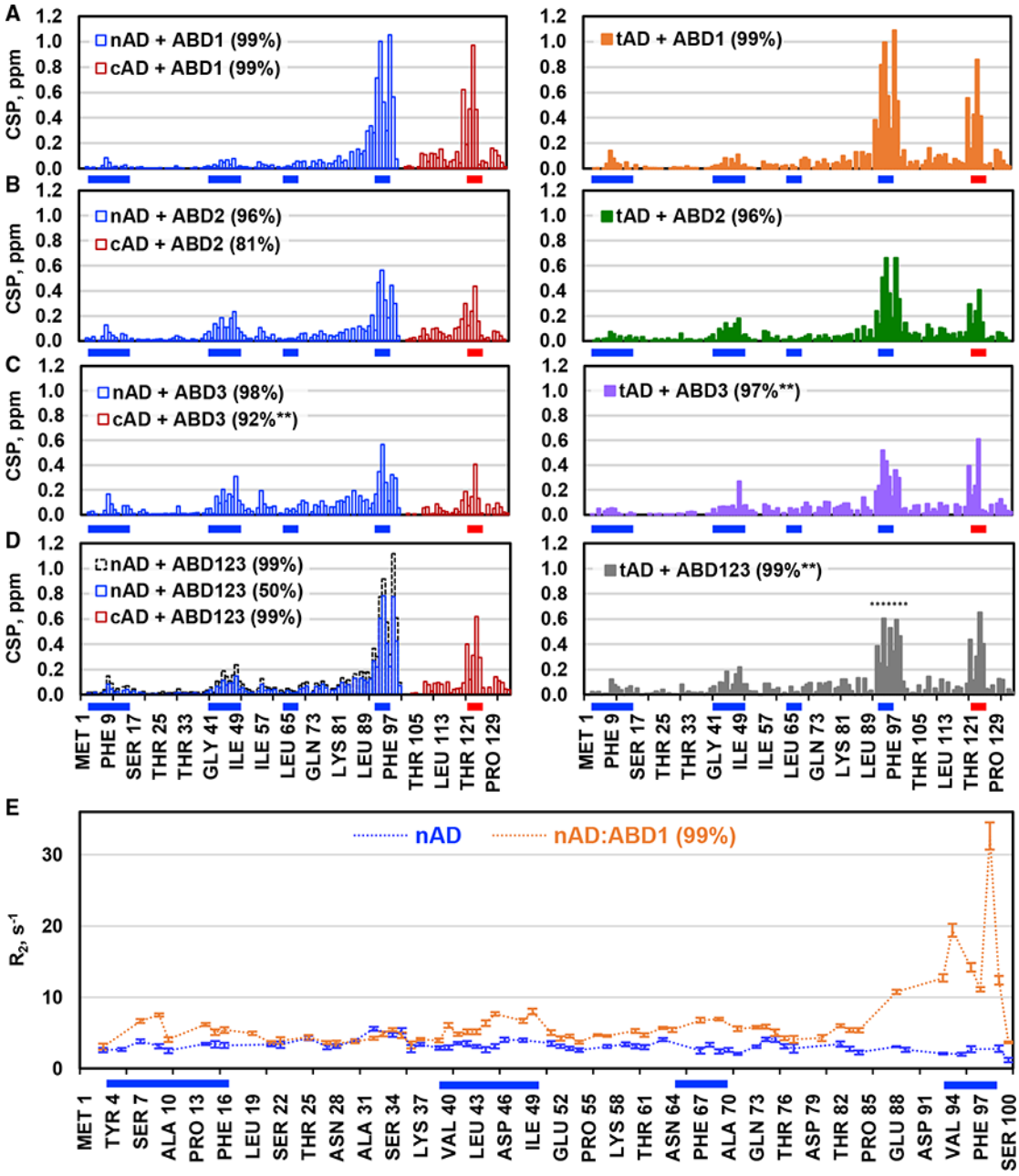

Figure 2. Gcn4 nAD and cAD Independently Interact with Med15 ABDs

(A–D) The NH chemical shift perturbation (CSP) of Gcn4 upon addition of Med15 ABD1 (A), ADB2 (B), ABD3 (C), or ABD123 (D). For each ABD, nAD and cAD regions have similar CSPs as independent regions (left) or in the context of full-length tAD 1–134 (right). See Figure S2 for (^{1}H,^{15}N)-HSQC titration spectra.

(C) Many cAD region peaks are lost after ~50% saturation for both the cAD + ABD3 and tAD + ABD3 titrations.

(D) HSQC peaks for tAD residues 91–99 of the tAD + ABD123 titration are lost at saturation levels >50%, so CSPs for nAD + ABD123 are also shown at 50% saturation for comparison; dashed black lines show full saturation data for nAD+ABD123 in (D). In all

panels, ** indicates situations where not all peaks trajectories could be followed to complete saturation.

(E) Backbone dynamics of nAD free (blue) and bound to ABD1 (orange). Increase of R_2 in nAD:ABD1 for each of the hydrophobic clusters suggests direct interaction of these regions with ABD1. Hydrophobic regions are highlighted by blue (nAD) and red (cAD) bars beneath each plot.

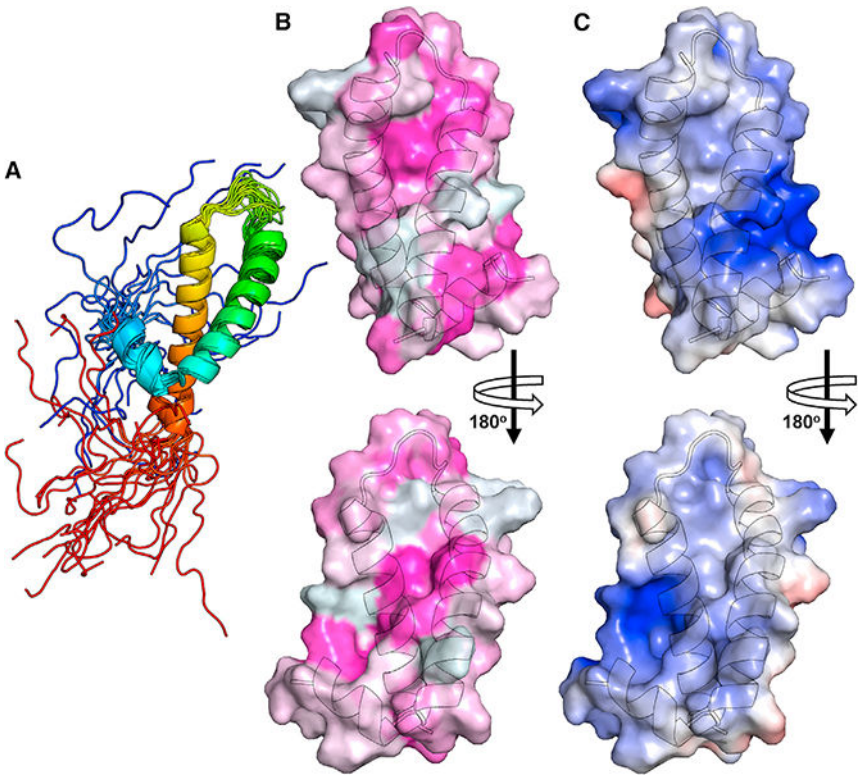

Figure 3. Structure and Surface Properties of Med15 ABD2

(A) The 20 lowest energy structures colored blue to red from the N to C termini.

(B and C) Hydrophobic (B; magenta) and electrostatic (C; red, <−5.0 kT/e; blue, >5.0 kT/e) surfaces plotted for the front side and back side of ABD2. Disordered N and C termini are not shown for surface representations. Electrostatic surfaces were generated using PDB2QPR and the APBS tool in pymol (Dolinsky et al., 2004). Hydrophobic surfaces are colored from magenta (most hydrophobic) to white according to the Eisenberg hydrophobicity scale.

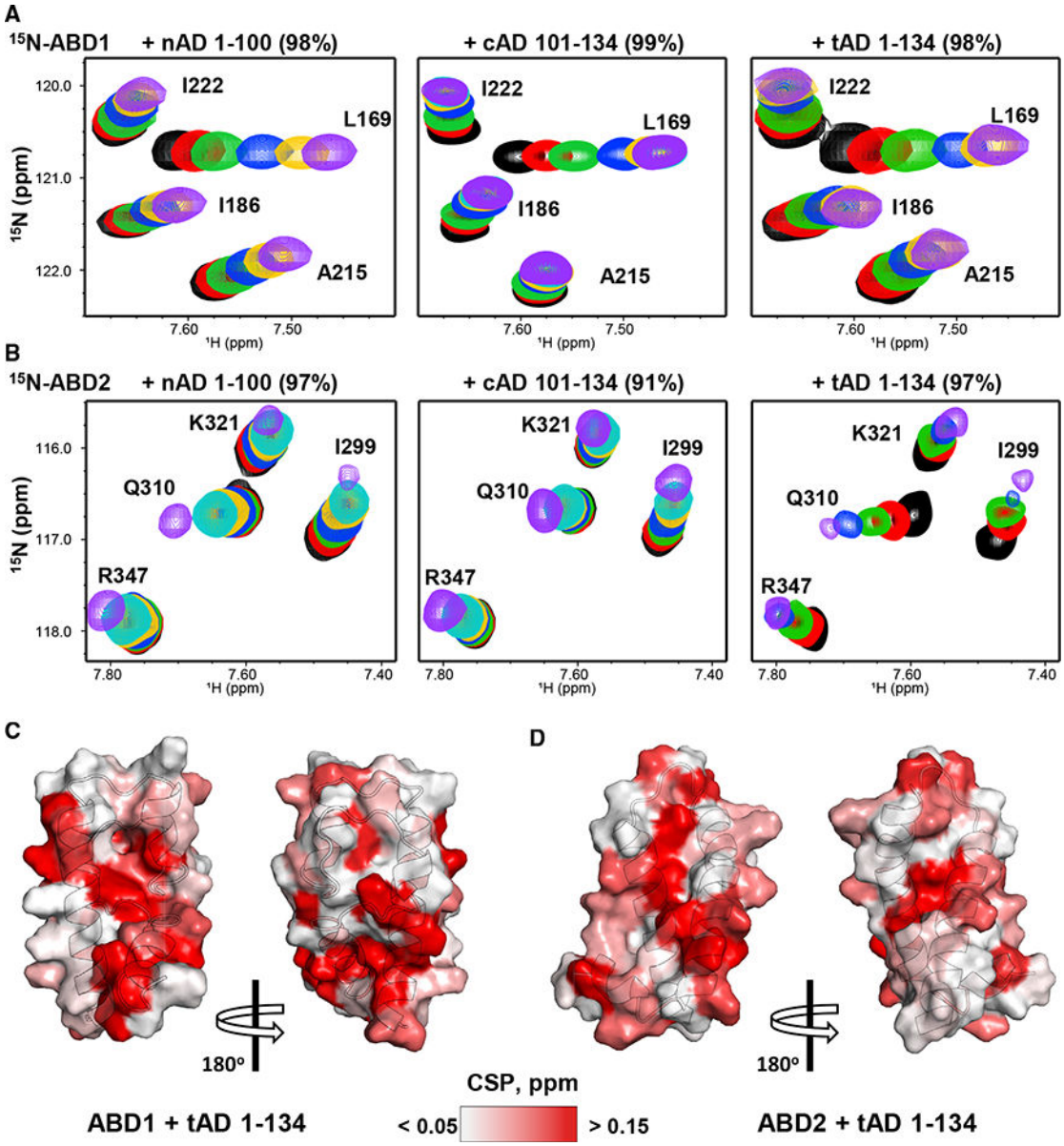

Figure 4. Med15 ABDs Show Widespread and Similar CSPs with Each Gcn4 AD

(A and B) Expanded region of the (^{1}H,^{15}N)-HSQC titration spectra of ABD1 (A) and ABD2 (B) with Gcn4 nAD, cAD, and tAD. Both ABD1 and ABD2 show very similar chemical shift trajectories whether nAD (left), cAD (middle), or tAD (right) is added. Values in parentheses are the percent saturation at the endpoint (purple spectrum).

(C and D) The CSPs of ABD1 + tAD (C) and ABD2 + tAD (D) plotted on the structures of ABD1 (2LPB) and ABD2 (6ALY), respectively. A redder surface color indicates a larger CSP.

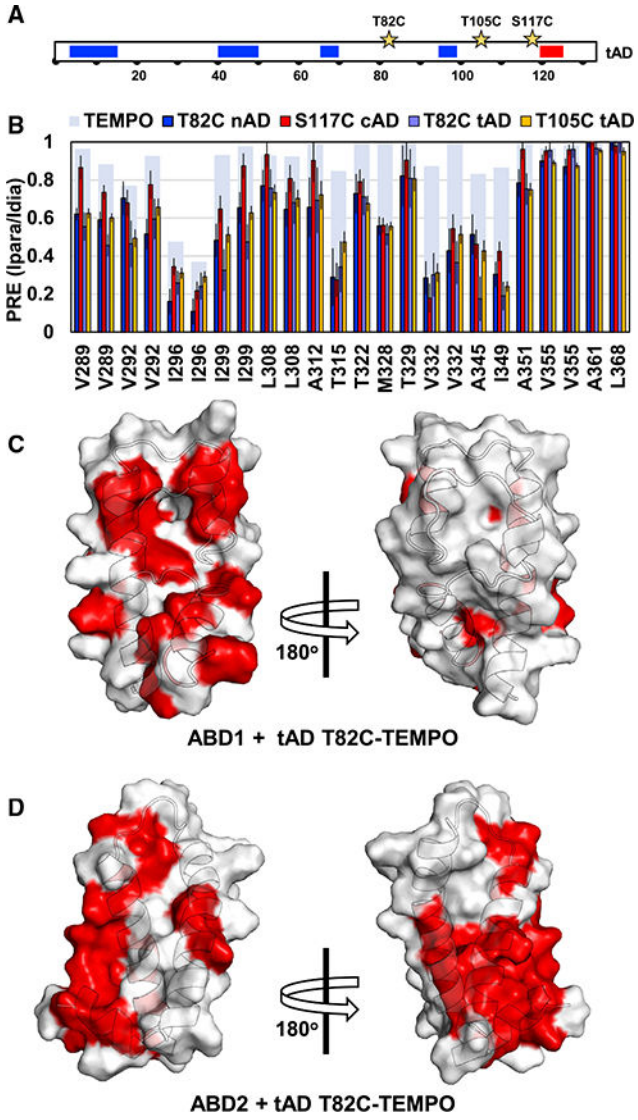

Figure 5. Paramagnetic Relaxation Enhancement Experiments of AD:ABD Complexes

(A) Spin label was attached at either side of the main clusters of nAD, cAD, and tAD (position indicated by a star).

(B) Each spin-labeled AD causes similar peak intensity loss at ABD2 (shown here for CH groups) and at ABD1 (see Figure S6 for NH and CH results). The results of a control experiment of ABD2 + free TEMPO are shown as light blue bars (see also Figure S6F).

(C and D) Surface plots for ABD1 + tAD T82C-TEMPO (C) and ABD2 + tAD T82C-TEMPO (D). Residues are colored red if the amide PRE < 0.7 or CH group PRE < 0.6.

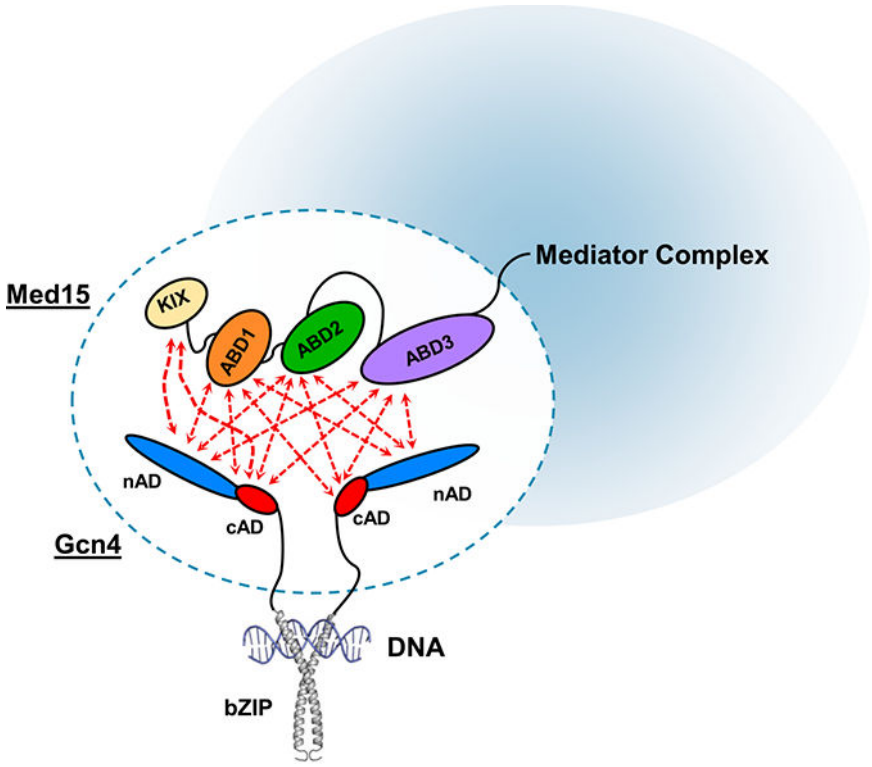

Figure 6. Model of the Fuzzy Gcn4-Med15 Complex

Transient fuzzy interactions of nAD and cAD with Med15 ABD subunits allows for significant contributions from even the weakest interacting parts by reducing the probability of total dissociation of Gcn4 tAD from Med15. Gcn4 bZIP and DNA structure from PDB: 1DGC are shown.

Table 1

Affinity of Gcn4 ADs for Med15 Activator-Binding Domains

ITC Binding Data					
Med15	**Gcn4**	**K_d (μM)**	**ΔH (cal/mol)**	**ΔS (cal/mol/deg)**	**Reference**
ABD1	nAD	10.8 ± 1.5	2,454 ± 78	31.0	
	cAD	10.1 ± 1.4	5,394 ± 150	4.58	(Brzovic et al., 2011)
ABD2	nAD	unable to measure			
	cAD	unable to measure			
ABD3	nAD	23.9 ± 2.0	7,015 ± 221	v	
	cAD	unable to measure			
FP Binding Data					
Med15	Gcn4	K_d (μM)			Reference
ABD1	nAD	3.3 ± 0.5			(Herbig et al., 2010)
	cAD	2.5 ± 0.4			(Herbig et al., 2010)
	tAD	2.66 ± 0.22			
ABD2	nAD	21.8 ± 3.8			(Herbig et al., 2010)
	cAD	147 ± 30			(Herbig et al., 2010)
	tAD	19.5 ± 2.74			
ABD3	nAD	2.6 ± 0.4			(Herbig et al., 2010)
	cAD	13.9 ± 0.5			
	tAD	4.40 ± 0.49			
KIX	nAD	unable to measure			(Herbig et al., 2010)
	cAD	unable to measure			(Herbig et al., 2010)
	tAD	unable to measure			
ABD123	nAD	0.36 ± 0.02			(Herbig et al., 2010)
	cAD	1.7 ± 0.1			(Herbig et al., 2010)
	tAD	0.109 ± 0.012			
KIX123	tAD	0.083 ± 0.009			